Matched Filter Cyclone Maximum Wind Retrievals Using CYGNSS: Progress Update and Error Analysis

Mohammad M. Al-Khaldi, *Member, IEEE*, Stephen J. Katzberg, Joel T. Johnson, *Fellow, IEEE*, Younghun Kang, Ethan J. Kubatko, and Scott Gleason, *Senior Member, IEEE*

***Abstract*—This article describes progress relating to a previously reported matched filter retrieval approach for the estimation of hurricane maximum winds using delay Doppler map (DDM) measurements of the Cyclone Global Navigation Satellite System (CYGNSS) mission. The retrievals presented are based on comparisons of these measured DDMs, and their simulated counterparts as a set of storm parameters are varied. The analysis presented examines the dependencies of retrieval performance on the synthetic storm model used as part of the forward modeling process using a set of CYGNSS storm-observing full DDM downlinks containing 68 tracks and spanning 18 storms over the period 2017–2020. Based on the combined use of multiple parametric storm models, retrieved hurricane maximum wind speed estimates showed correlations of 92%, root-mean-square error (RMSE) of 6.05 m/s, unbiased RMSE of 6.05 m/s, mean difference of 4.83 m/s, and a bias of 0.09 m/s relative to reference data. Mean retrieval error relative to storm maximum wind is 11.11%. The dependence of retrieval error on measurement maximum delay extent is also analyzed using CYGNSS Raw I/F downlinks, from which a significant near-monotonic decrease in retrieval errors is observed as the delay extent of the measurement is increased. The analysis presented in this work highlights the potential for using matched filter retrieval methodologies for cyclone wind speed estimation in spaceborne Global Navigation Satellite Systems Reflectometry systems.**

***Index Terms*—Bistatic radar systems, Cyclone Global Navigation Satellite System (CYGNSS), global navigation satellite systems reflectometry (GNSS-R), remote sensing, sea surface scatter, tropical cyclones.**

I. Introduction

CYCLONES are among the most destructive naturally occurring phenomena, posing threats to life as they make landfall and economic damage through destruction of property. These factors motivate the analysis and tracking of cyclone characteristics as they undergo various levels of development. The ability to do so, however, is complicated by the fact that cyclones undergo much of their development in the open ocean [1] at considerable distances from coastal regions, thereby minimizing the ability to study them through direct reconnaissance.

The global coverage of spaceborne platforms and the sensitivity of their measurements to various storm properties has motivated the use of a wide range of sensors, including the Special Sensor Microwave Imager/Sounder, Geostationary Operational Environmental Satellite system, Quick Scatterometer, and Advanced Scatterometer [2]–[5] as a means of mitigating the scarcity of cyclone data over the ocean. The utility of these observations is nonetheless limited by their sparse revisits and sensitivity to cloud cover and heavy rain that typically prevails around a cyclone's central core. In contrast, Global Navigation Satellite System Reflectometry (GNSS-R) as an emerging spaceborne remote sensing technique [6], [7] offers to bypass many of these limitations. The sensitivity of GNSS-R measurements to a wide range of storm properties has been previously illustrated using the technology demonstration satellite 1 (TDS-1) [8] and more recently using the Cyclone Global Navigation Satellite System (CYGNSS) constellation [9], [10] through the use of the satellites' respective surface wind speed estimates with temporal revisits ranging between 3 and 7 h [11], [12]. The usefulness of their measurements for the analysis of storm properties motivates further development of a previously reported "matched filter" hurricane maximum wind retrieval approach [13], [14].

This work examines an expanded CYGNSS dataset as compared to [13] and [14], including 18 storms throughout the 2017–2020 analysis period. Particular emphasis is placed on the storm models used as part of the algorithm's forward modeling process, and a strategy is presented through which CYGNSS retrieval performance may be optimized based on the combined use of multiple storm models. Because the proposed methodology bases its estimates on delay Doppler map (DDM) "shape," error dependencies on the measurements' delay extent are also analyzed.

The rest of this article is organized as follows. Section II provides an overview of CYGNSS's basic operation, its standard products used for wind speed estimation, and its special acquisition modes, including Full DDM and Raw I/F downlinks, relevant for matched filter hurricane maximum wind speed estimates. Section III provides a brief overview of the matched

Manuscript received November 28, 2020; revised February 19, 2021; accepted March 9, 2021. Date of publication March 17, 2021; date of current version April 7, 2021. This work was supported in part by the NASA ROSES 2018 CYGNSS Competed Science Team under Grant 80NSSC18K0712 and in part by an allocation of computing resources from the Ohio Supercomputer Center. *(Corresponding author: Mohammad M. Al-Khaldi.)*

Mohammad M. Al-Khaldi and Scott Gleason are with the Constellation Observing System for Meteorology, Ionosphere, and Climate Program, University Corporation for Atmospheric Research, Boulder, CO 80301 USA (e-mail: malkhaldi@ucar.edu; gleason@ucar.edu).

Stephen J. Katzberg is with the NASA's Langley Research Center, Hampton, VA 23666 USA, and also with the South Carolina State University, Orangeburg, SC 29117 USA (e-mail: stephen.j.katzberg@nasa.gov).

Joel T. Johnson is with the Department of Electrical and Computer Engineering and the ElectroScience Laboratory, The Ohio State University, Columbus, OH 43210 USA (e-mail: johnson.1374@osu.edu).

Younghun Kang and Ethan J. Kubatko are with the Department of Civil, Environmental and Geodetic Engineering and the Computational Hydrodynamics and Informatics Laboratory, The Ohio State University, Columbus, OH 43210 USA (e-mail: kang.1049@osu.edu; kubatko.3@osu.edu).

Digital Object Identifier 10.1109/JSTARS.2021.3066406

filter retrieval approach and maximum wind estimators. Section IV then provides an overview of the basic storm parametric functions, whose combined use forms the basis for the retrieval strategy presented in this work. Section V reports results, errors, and their dependencies on synthetic storm models, the level of storm development, and the measurement delay extent. Recommendations for future work are provided in Section VI.

II. Background

The CYGNSS constellation includes eight receivers in low Earth orbit, each with a delay Doppler mapping instrument [15] as the primary payload. The cross correlation of scattered GPS transmissions off the Earth's surface with internally generated C/A code replicas results in a mapping of received power from the spatial domain to delay Doppler space, giving rise to the fundamental GNSS-R measurement, the DDM. The standard CYGNSS Level-1 DDMs are cropped from a larger Full DDM formed on board the receivers and spans a maximum delay extent of ≈3.5 chips (17 delay bins at ≈0.25 μs chip sampling). This standard product forms the basis for Level-2 wind speed estimates [16], [17].

Level 2 data emphasize the conversion of quantities derived from Level-1 DDMs to ungridded wind speed and mean square slope estimates. To do this, the normalized radar cross section (NRCS) is derived from DDMs using the delay Doppler map average (DDMA) [16], [17] defined as an integration of the bistatic radar cross section within a predefined delay Doppler window about the specular DDM bin normalized by the effective scattering area. The standard wind speed product also uses a leading edge slope (LES) quantity. Both the DDMA and the LES are regressed against wind speeds provided by other instruments and/or models to derive a geophysical model function (GMF). At a fundamental level, the GMF is, therefore, a function that accepts an NRCS or a related observable quantity as its input and provides wind speed estimates as its output. For a more comprehensive overview, see [18].

While CYGNSS's retrievals continue to undergo various stages of development and improvement, including storm centric remapping of surface winds [21], trackwise debiasing of CYGNSS products [22], [23], and more sophisticated calibration/quality control practices [24]–[27], a number of factors currently limit the efficacy of standard GMF-based approaches in successfully characterizing cyclone maximum winds using spaceborne GNSS-R systems.

This includes the tendency of received power to decrease monotonically at a slow rate with high surface wind speeds, characteristic of cyclones, such that a saturation effect takes place at surface winds beyond ≈30 m/s with the slope of the line relating received power to surface wind approaching zero. As a result, the sensitivity to surface winds is reduced. Furthermore, the reliance on the magnitude of CYGNSS observables makes them susceptible to calibration uncertainties and necessitates accurate absolute power calibration for reflections associated with 32 GPS transmitters and eight CYGNSS receivers. This is further complicated by the fact that Level-2 winds are derived from Level-1 DDMs having limited spatial extent such that CYGNSS tracks need to be within close proximity to storm centers to allow for GMF methodologies to be effective. These considerations motivate the continued development of matched filter retrievals, described in the next section, as a means of bypassing many of these limitations.

III. Matched Filter Retrieval Approach Overview

The "matched filter" hurricane maximum wind retrieval approach is based on estimating a set of hurricane parameters based on maximum "likeness" between a track of measured $M(\tau, f_D; V_{\max})$ and simulated $S(\tau, f_D; V_{\max})$ DDMs, both normalized by their rms amplitudes, where $V_{\max}$ represents the cyclone maximum wind speed.

The simulated DDMs are produced over the range $20 \leq V_{\max} \leq 80$ m/s at 1-m/s increments based on a set of GPS/CYGNSS geometries that are within a 200-km radius of a given storm's center at the time of CYGNSS's observation. Simulated DDMs are produced using an end-to-end (E2ES) forward model [28], [29]. Predictions of received power within a DDM's delay Doppler bin are based on the bistatic radar equation [7] with surface wind roughening effects accounted for through empirically determined estimates of mean square slopes [30], [31]. The E2ES is used to produce a reference library of DDMs under a variety of storm conditions and storm center locations that is used as part of the retrieval process.

Because hurricane structures result in nonuniform surface winds, the E2ES functionality was extended to include a set of synthetic storm models, whose generation is based on parametric wind relationships. The studies of [14] have previously discussed the impacts of incorporating synthetic storm models, relative to uniform surface winds, on reference DDM "shapes." The "likeness" of the E2ES predictions and CYGNSS measurements for storm observing tracks is based on two maximum wind $V_{\max}$ estimators seeking to maximize correlations as in (1) and (2) and minimizing their root-mean-square errors (RMSE) as in (3) over a track of P specular points

$$V_{\max}^{*} = \underset{V_{\max}}{\operatorname{argmax}} \sum_{p=1}^{P} R\left(V_{\max}\right) \tag{1}$$

where

$$R\left(V_{\max}\right) = \frac{\left|\left\langle M_p^{\tau,f_D}(V_{\max}), S_p^{\tau,f_D}(V_{\max})\right\rangle\right|^2}{\left\langle M_p^{\tau,f_D}(V_{\max}), M_p^{\tau,f_D}(V_{\max})\right\rangle \left\langle S_p^{\tau,f_D}(V_{\max}), S_p^{\tau,f_D}(V_{\max})\right\rangle} \tag{2}$$

in which the bracket notation refers to a pointwise multiplication of DDM "pixels" followed by a summation of all pixel products, excluding noise-only delay rows

$$V_{\max}^{*} = \underset{V_{\max}}{\operatorname{argmin}} \sum_{p=1}^{P} \sqrt{\frac{1}{N\tau}\frac{1}{N_f}\sum_{i=1}^{N_\tau}\sum_{j=1}^{N_f}\left|M_p(\tau^i, f_D^j; V_{\max}) - S_p(\tau^i, f_D^j; V_{\max})\right|^2} \tag{3}$$

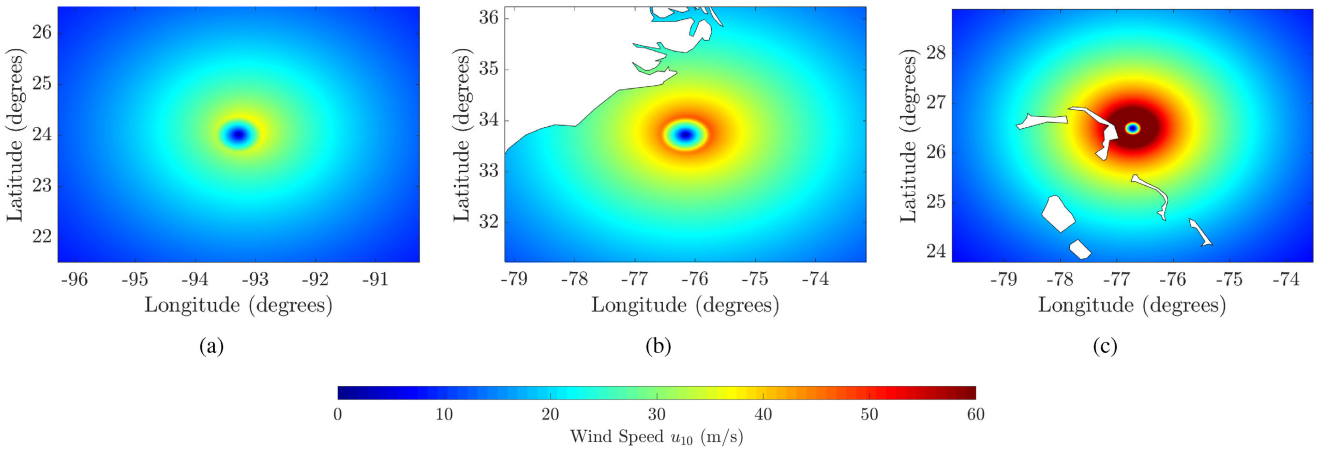

Fig. 1. Willoughby renditions of storms for which standard and special CYGNSS downlinks have been made available. (a) Harvey on DOY 236, 2017. (b) Florence on DOY 256, 2018. (c) Dorian on DOY 244, 2019. Areas in white are land.

where N_τ and N_f and the total number of delay and Doppler bins in a single DDM, respectively.

The final retrieved maximum wind value is the average of the solutions to (1) and (3).

IV. Synthetic Storm Models

A. Willoughby Model

A wide range of synthetic storm models have been proposed in the literature [32]–[37]; the choice of which model(s) to explore is dictated by the need for computational efficiency of the model implementation while ensuring that it describes a realistic storm structure. The reported improvement that the Willoughby storm [38], [39] has achieved over preceding models in [13] has motivated its use in initial investigations [13], [14] as it facilitates a reasonable compromise between these goals.

The model is a function of storm latitude φ and sustained surface wind (SSW) V_{max} and has been shown to outperform preceding models such as those in [35] and [32], as shown in [38] and [39].

The Willoughby model divides descriptions of tropical cyclone surface winds into three domains. The first V_{in} describes winds within the eyewall radius given by

$$V_{\text{in}} = V_{\text{max}} \left(\frac{r}{R_{\text{max}}} \right)^n \tag{4}$$

where r is the radial separation from a surface point to storm center, n is an empirical fit "power" parameter, and R_{max} is the radius of maximum winds. The second domain V_{out} describes surface winds beyond the transitional region, the region between the eyewall and the "steady-state" background wind field, and is given by

$$V_{\text{out}} = V_{\text{max}} \left[(1-A) e^{-\frac{r-R_{\text{max}}}{X_1}} + A e^{-\frac{r-R_{\text{max}}}{X_2}} \right] \tag{5}$$

where $A \geq 0$ is a mixing weight factor, X_1 is a decay length constant, and X_2 is the outer vortex length of decay. The winds within the third, transitional, region V_{tr} are a weighted mixture of the winds in the inner and outer domains

$$V_{\text{tr}} = V_{\text{in}}(1-\omega) + \omega V_{\text{out}} \tag{6}$$

where ω is the weighting mixing factor. The parameters $R_{\text{max}}, n, X_1, X_2, A$, and ω are all described by empirical fits expressed as a function of storm V_{max} and storm latitude φ [38], [39]. The Willoughby model is azimuthally symmetric, but extensions may be incorporated to its model functions to introduce some level of asymmetry about its eyewall, using (7), which entails incorporating storm translational speed (ground speed in direction of propagation) and translational direction (heading, measured in degrees clockwise from north) [13]

$$V_f = \sqrt{(-V_m \cos\theta_t)^2 + \left[\frac{V_t \sin\theta_t}{R_{\text{max}}^2 + r^2} \right]^2} \tag{7}$$

where V_f is the final model description of surface wind, V_m is the output wind using the three model functions, θ_t is the storm's translational direction, and V_t is its translational speed. Example Willoughby renditions of hurricanes observed by the CYGNSS constellation are depicted in Fig. 1.

B. Generalized Asymmetric Holland Model

The E2ES has also been extended to include a second synthetic storm model, the Generalized Asymmetric Holland Model (GAHM) [40]. The GAHM is a quadrant specific generalization of the 1980 Holland model, in which storm profiles are described by parametric relationships given by rectangular hyperbolas scaled by shape and location parameters. This allows for the introduction of true asymmetries within the storm profile, in contrast to the Willoughby model. Comparisons between the two will be used for the assessment of the sensitivity of the retrieval approach to the employed storm model.

The GAHM divides the storm into four quadrants each with three isotachs (i.e., contours of constants wind values at varying radial separations from the storm center). The model describes the storm using surface wind values in 12 different regimes. To

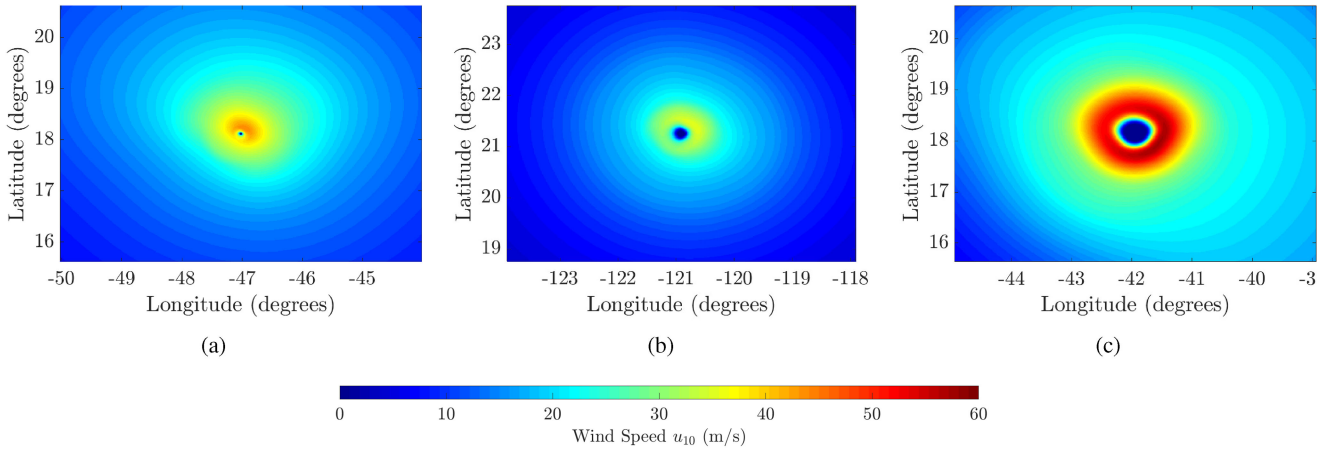

Fig. 2. GAHM renditions of storms for which standard and special CYGNSS downlinks have been made available. (a) Irma on DOY 246, 2017. (b) Dorian on DOY 248, 2019. (c) Lorenzo on DOY 270, 2019.

do this, the parameters Ψ_g and B_g are defined as

$$\Psi_g = 1 + \frac{V_{\max} R_{\max} f}{B_g \left(V_{\max}^2 + V_{\max} R_{\max} f\right)} \tag{8}$$

$$B_g = \frac{\left(V_{\max}^2 + V_{\max} R_{\max} f\right) \rho e^{\Psi}}{\Psi \left(P_n - P_c\right)} \tag{9}$$

and the surface wind V_g and pressure P_g fields are then given by

$$V_g(r) = \Bigg(\left(V_{\max}^2 + V_{\max} R_{\max} f\right) e^{\Psi(1 - R_{\max}/r)^B} \times \left(\frac{R_{\max}}{r}\right)^B + \left(\frac{rf}{2}\right)^2 \Bigg)^{1/2} - \left(\frac{rf}{2}\right) \tag{10}$$

$$P_g(r) = P_c + \left(P_n - P_c\right) e^{-\Psi(R_{\max}/r)^B} \tag{11}$$

with

$$B = \frac{V_{\max}^2 \rho e}{P_n - P_c} \tag{12}$$

where B is the Holland-B parameter describing the overall shape of surface wind contours within a given domain, B_g is the adjusted Holland-B parameter, P_c is the storm's central pressure, P_n is its ambient pressure, Ψ_g is a scale factor, and ρ is the density of air. The parameter f is the Coriolis force and is given by

$$f = \frac{2\pi}{86\,164} \sin(\varphi). \tag{13}$$

The coupled nature of the GAHM functions requires iterative determination of the parameters Ψ_g and B_g that results in radial conditions dictated by the radius of maximum winds and isotach radii within each of the four quadrants. This also requires, as inputs, additional ancillary information pertaining to storm structure obtained from National Hurricane Center Best Track forecasts. It is noted that depending on a given storm's structure, both the Willoughby model and the GAHM predict a nonphysical near-zero wind field distribution near its center. In this work, the implementation of parametric storm models in the E2ES is such that within the eyewall, model wind estimates are overridden and set to a constant 7.5 m/s value if they fall below this cutoff value. Comparisons between the ancillary information required by the Willoughby model and the GAHM, as a function of level of storm development, are summarized in Table I.

TABLE I
ANCILLARY PARAMETERS REQUIRED TO IMPLEMENT THE GAHM AND THE WILLOUGHBY MODEL AS PART OF THE E2ES FORWARD MODELING PROCEDURE

GAHM	Willoughby
Storm center latitude	Storm center latitude
Storm center longitude	Storm center longitude
Minimum sea level pressure	-
Pressure of the last closed isobar	-
Radius of maximum winds	-
Radius in quadrant 1 at 34kt isotach	-
Radius in quadrant 2 at 34kt isotach	-
Radius in quadrant 3 at 34kt isotach	-
Radius in quadrant 4 at 34kt isotach	-
*Radius in quadrant 1 at 50kt isotach	-
*Radius in quadrant 2 at 50kt isotach	-
*Radius in quadrant 3 at 50kt isotach	-
*Radius in quadrant 4 at 50kt isotach	-
*Radius in quadrant 1 at 64kt isotach	-
*Radius in quadrant 2 at 64kt isotach	-
*Radius in quadrant 3 at 64kt isotach	-
*Radius in quadrant 4 at 64kt isotach	-

Asterisk indicates that need for parameter is contingent on level of storm development.

The more sophisticated nature of the GAHM storm model adds complexity to the forward modeling process, but provides the advantage of producing significantly more realistic renditions of synthetic storms. Examples of this are shown in Fig. 2 for three storms for which the CYGNSS constellation provided downlinks under its standard and special modes of operation. The contrasts between this and the Willoughby renditions in Fig. 1 are readily identifiable, where significant distortions and asymmetries varying from one storm quadrant to another mimicking realistic storm behaviors are observed. The GAHM provides this more realistic description of storm structure at the expense of additional ancillary data, here obtained from

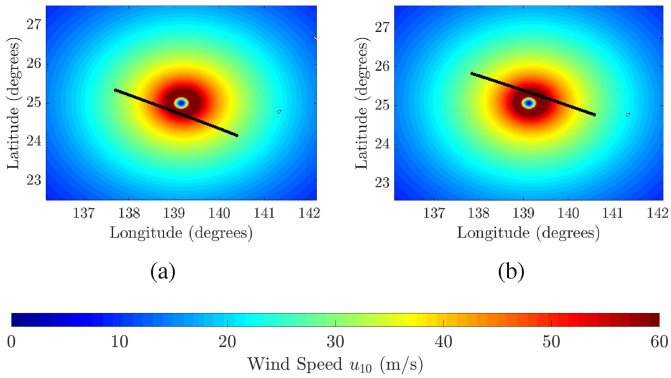

Fig. 3. Retrieval results for two colocated tracks overlooking Typhoon Hagabis on DOY 283, 2019. (a) Willoughby rendition of storm based on track 1 with $V_{\max} = 70$ m/s retrieval value. (b) Willoughby rendition of storm based on track 2 with $V_{\max} = 70$ m/s retrieval value. Locations of CYGNSS's specular points are indicated by the black scatters.

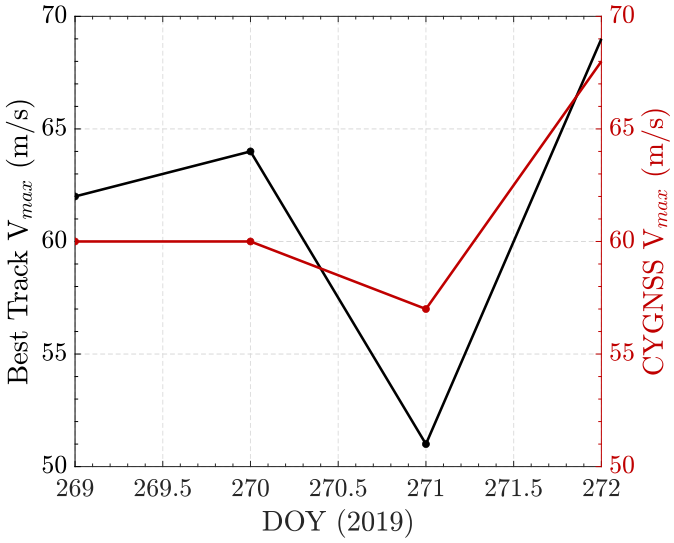

Fig. 4. Retrieval results across four days of Hurricane Lorenzo's life cycle.

the Best Track database. In the results to be shown, all the ancillary information of Table I (which, of course, excludes storm maximum winds) is used as part of the retrieval. It is noted that some of the ancillary information required (such as the presence of various isotachs) is correlated with the maximum wind speed. However, studies of the retrieval process showed that the ancillary parameters alone still allow a wide range of maximum wind speeds in the storm model, so that the retrievals to be shown contribute distinct information on storm maximum winds. The impact of the GAHM on the retrieval process is explored further in Section V.

V. Analysis

A. Full-DDM-Based Retrievals Using Willoughby

The studies of [14] have previously reported successful Full-DDM-based matched filtered retrievals, with mean difference Δ_{mean} on the order of $\approx$5 m/s, using the Willoughby model as part of the forward modeling process over a limited data record.

Beyond retrieval errors, two other considerations in the assessment of the approach's effectiveness are of particular interest. The first relates to the need for consistency in retrievals over periods for which a given storm is not expected to have evolved, developed, or dissipated in any substantial manner. An opportunity to examine the consistency of the retrieval methodology is afforded by observations of the same storm within relatively short time spans. While the occurrence of such scenarios is uncommon, Full DDM downlinks made for tracks observing Typhoon Hagibis in 2019 made this possible.

Typhoon Hagabis was among the most devastating pacific storms on record, starting as a tropical depression in the Pacific Ocean and developing into a category 5 super typhoon inflicting significant damage to Guam, the Mariana Islands, and Japan. Numerous full DDM downlinks were made for tracks observing Typhoon Hagibis, but those made on DOY 283-2019 depicted in Fig. 3 were of most interest. The two were made in tandem, approximately 20 min apart, both roughly 20 km on opposite sides of the storm center. A test of retrieval consistency in this case requires that the two retrievals have very small or zero differences. The retrieved storm profiles using the Willoughby model for both tracks are depicted in Fig. 3.

Both tracks were associated with an identical retrieval value of $V_{\max} = 70$ m/s; relative to the reported 71.5 m/s truth $V_{\max}$ value, both results correspond to an error of 1.5 m/s or equivalently 2.14% relative to storm $V_{\max}$. As a result, the retrieval methodology for this case study passes both the consistency and low error ($\Delta < 10\%$) requirements. The consistency between the two retrievals is also attributed, in part, to the symmetry of Typhoon Hagibis's structure. Here, it is noted that all reference $V_{\max}$ estimates are interpolated between two known values (reported over 6-h intervals) to values that correspond to the mean CYGNSS along track timestamp.

The second consideration relates to the responsiveness of both the CYGNSS measurements and the retrieval methodology to various levels of storm development. Due to the infrequent availability of Full DDM measurements, it is often the case that retrievals capture a single snapshot of the storm's behavior during a single instant of the storm's life cycle offering little insight to its growth and decay. Full DDM downlinks for Hurricane Lorenzo, however, were made available over four consecutive days during 2019. Retrieval results are depicted in Fig. 4, where it can be observed that the storm's $V_{\max}$ behavior was such that it underwent an initial period of growth, then decay, followed by another growth phase. A response to these tendencies is clearly captured within the Full DDM measurements and successfully translated through the matched filter retrieval methodology to successful $V_{\max}$ retrievals, where over the four-day period, mean retrieval error was $\Delta_{\text{mean}} = 3.25$ m/s.

While the results of the retrieval process using the Willoughby model indicate satisfactory performance, tests of retrieval errors associated with weaker storms showed significantly higher error levels. An example of this is explored in Fig. 5, where an attempted retrieval for a Full DDM track overlooking hurricane Harvey on DOY 236, 2017 was found to be associated with a significant overestimation of retrieved $V_{\max}$ of 25 m/s.

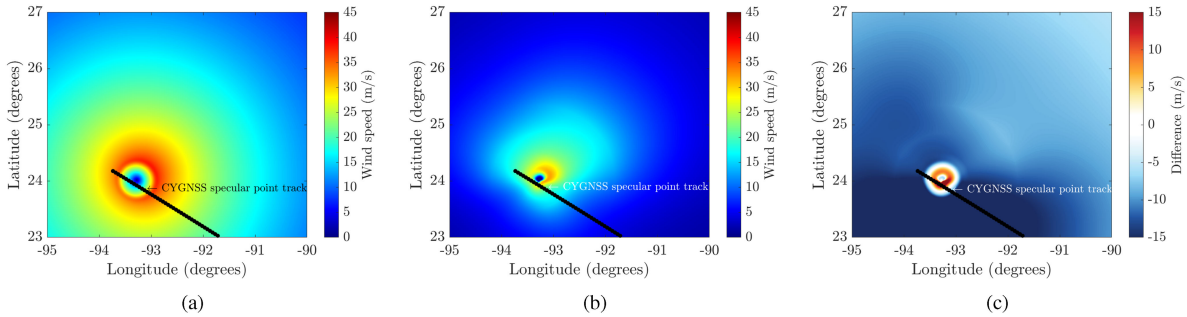

Fig. 5. Synthetic storm model descriptions of surface winds based on Best Track $V_{\max} = 36$ m/s for hurricane Harvey on DOY-Year 236-2017. (a) Using the Willoughby model, whose use resulted in an ≈25 m/s $V_{\max}$ error relative to Best Track. (b) Using the GAHM, whose use resulted in an ≈5 m/s $V_{\max}$ error relative to Best Track. (c) Difference in surface wind distributions between the two models.

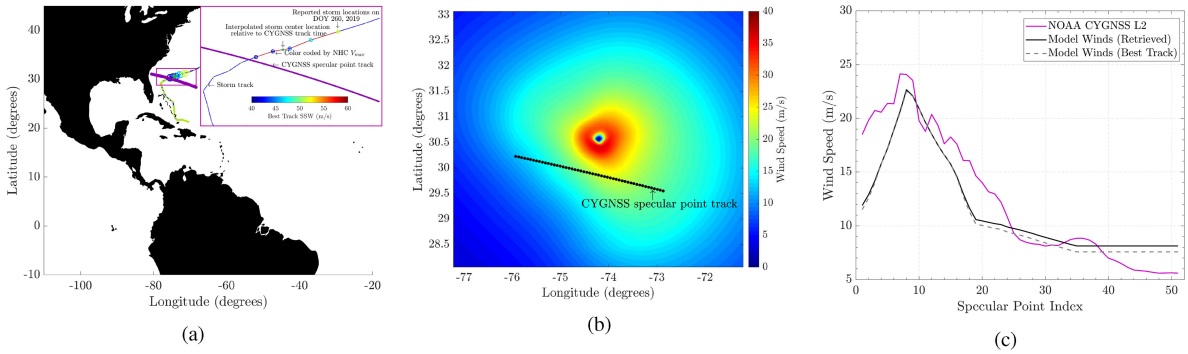

Fig. 6. (a) Hurricane Humberto and CYGNSS track on DOY 260, 2019. (b) Synthetic storm based on the GAHM and retrieved storm $V_{\max}$ using CYGNSS Full DDMs. (c) Local wind profile.

These increased error levels are expected to be in large part attributable to the inability of the Willoughby model to describe storm structure with lower levels of development with sufficient accuracy. The results depicted in Fig. 5 clearly highlight the importance of the parametric storm model providing an accurate representation of the storm structure. While the Willoughby model is known to outperform some descriptions, it is also known to have a tendency to overestimate surface wind speeds at greater distances from the storm center [14]. Furthermore, while azimuthal asymmetries are included in the model used through the incorporation of translational speed/direction, the changes do not introduce large quadrant specific variations across the various storm radii (R_{64}, R_{50}, and R_{34}). This motivates exploring the combined use of the Willoughby model with more sophisticated models like GAHM to account for these effects. This is explored in the next section.

B. *Full-DDM-Based Retrievals Using GAHM*

For the cases shown in Fig. 5, variations in storm structure are readily identifiable, where it can be observed that the GAHM is significantly more "contained," whereas Willoughby suggests noticeably higher wind speeds at distances farther than 50 km from the storm center. Furthermore, through ingesting Best Track forecast information pertaining to storm radii as part of its implementation, the GAHM is significantly more asymmetric compared to the Willoughby model and, as a consequence, results in significant changes in wind field distributions. Comparisons against Ocean Weather Inc. [41] wind fields suggests that the GAHM is more accurate in this case having an RMSE ≈2 m/s for surface winds within 250 km of the eyewall. Depending on location within the grid, local wind variations between the models, both generated based on a reference Best Track $V_{\max}$ estimate of 36 m/s, exceed 20 m/s. As a result, variations exceeding 15% based on implementations of the two storm models were noted within the "shape" of the reference DDMs. Retrieval errors were subsequently found to range between 5 m/s using GAHM and 25 m/s using Willoughby.

The success of the GAHM in describing weaker storms, and the implications this has in terms of retrievals with low errors, is not unique to hurricane Harvey and has been observed repeatedly throughout numerous attempted retrievals. For example, in Fig. 6, the retrieval is conducted for a track of CYGNSS Full DDMs during the 2019 Atlantic hurricane season overlooking hurricane Humberto.

During this time, Humberto was a category 2 hurricane with an interpolated Best Track $V_{\max}$ of ≈43 m/s. The retrieved $V_{\max}$ based on CYGNSS measurements was 40.5 m/s (an average of 40 m/s based on maximum R and 41 m/s based on minimum RMSE) suggesting an error of ≈2.5 m/s. Using the retrieved $V_{\max}$, coupled with *a priori* Best Track data, a complete storm profile was then constructed as shown in plot (b) using the GAHM.

As an additional step, the wind field grid in plot (b) can be sampled at the CYGNSS specular point locations to produce a local, along track profile of wind speeds that are compared against a version of CYGNSS L2 winds produced by the National Oceanic and Atmospheric Administration that underwent

TABLE II
RETRIEVAL RESULTS BASED ON CYGNSS FULL DDM OBSERVATIONS FOR STORMS WITH LOW LEVELS OF DEVELOPMENT AND USE OF THE GAHM AS PART OF THE FORWARD MODELING PROCEDURE

Track	DOY	Year	Storm	Storm Cat.	$\lvert\Delta_w\rvert$ (m/s)
1	237	2017	Harvey	2	2.84
2	280	2017	Nate	3	3.08
3	280	2017	Nate	3	3.08
3	255	2018	Florence	3	3.74
4	242	2019	Dorian	3	3.52
5	269	2019	Lorenzo	1	2.25

trackwise debiasing. The modest error levels with respect to the retrieved $V_{\max}$ together with the large extent of similarity between the two profiles are evidence of the success of the retrieval process where across the "retrieved" and the L2 wind profile RMSE was 2.73 m/s, unbiased RMSE (URMSE) was 2.45 m/s, and bias was 1.16 m/s. A high degree of correlation estimated at 92.7% is also noted. It is also shown that due to the minimum track to storm center separation of 75 km in this case, the 2.5-m/s difference in retrieved versus Best Track $V_{\max}$ difference did not result in appreciable variations in the local wind profiles across the two, as shown in plot (c). Examples of results from other retrieval attempts based on the use of the GAHM for weaker storms are summarized in Table II.

C. Full-DDM-Based Combined Retrievals

The retrieval successes using the GAHM for storms with low levels of development and Willoughby for storms with higher levels of development motivates their use as part of a combined $V_{\max}$ estimation strategy. Tests across a wide range of Full DDM downlinks suggest that optimal performance is achieved when the GAHM is used for storms with levels of development $D_s \leq 3$ and using the Willoughby model within the range $4 \leq D_s \leq 5$ on the Saffir–Simpson Hurricane Scale [43].

The results of this strategy are depicted in Fig. 7 for a total of 68 Full DDM retrievals spanning 18 storms over the period 2017–2020, where mean retrieval difference $\Delta_{\text{mean}} = 4.83$ m/s, RMSE = 6.05 m/s, URMSE = 6.05 m/s, bias 0.09 m/s, and overall correlation $R = 92\%$. Relative to storm $V_{\max}$, retrieval error was found to be on average 11.11%, highlighting the success of the retrieval methodology.

D. Analyzing Error Dependence on Measurement Delay Extent Using CYGNSS Raw I/F Downlinks

Other potential venues for improvement are explored in the context of measurement delay extent. An analysis extending the retrieval approach to standard Level-1 CYGNSS DDMs, motivated by their more frequent availability, has shown that varying storm $V_{\max}$ introduces limited "shape" changes to the 11×17 delay Doppler region, thereby resulting in a very "flat" response in correlation/RMSE across the varying wind speeds. As a consequence, this did not allow successful retrievals to be conducted using the standard DDMs. On the other hand, based on initial simulation results, a very clear decline in error is observed with increasing measurement delay extent owing

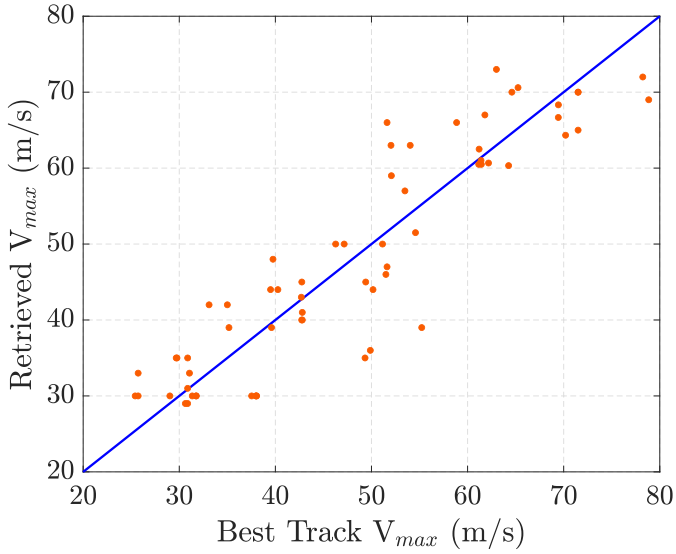

Fig. 7. Scatter plot of retrieved CYGNSS-based storm $V_{\max}$ results for 68 Full DDM tracks across 18 storms over the period 2017–2020 based on the combined use of the GAHM and the Willoughby model.

to the increased information this facilitates about the observed storm. The impact of conducting retrievals at increased delays is, therefore, explored further in the context of CYGNSS Raw I/F mode measurements.

The primary distinction between the different DDM products is their varying extents in delay. L1 DDMs are limited to a 3.5 chip maximum delay extent, Full DDMs are limited to 16 chips (although a special Full DDM mode with an increase delay extent is currently under consideration), and Raw I/F streams enable the creation of DDMs with an arbitrary maximum delay extent up to even 50 chips or more. An example of the surface footprint this translates to for a CYGNSS Raw I/F track observing hurricane Florence is depicted in Fig. 8(a). The increased delay extent of the Full DDM and Raw I/F modes is particularly advantageous from a retrieval perspective for a number of reasons. In observation scenarios where CYGNSS tracks do not align exactly with the storm center (i.e., "near miss" geometries) and instead pass through the storm at varying radial separations from its center, the effectiveness of the L1 DDM may be limited as it only furnishes information about a small portion of the storm. The increased spatial span of the special modes of acquisition enable spatial extents that instead "sample" a larger portion of the storm profile so that information from the storm center, transition region, and the portion of the storm that is beyond the transition region is included. The larger "wind variance" mapped within each footprint is shown in Fig. 8(b). As a result, measurements with increased delay extent hold the potential to improve retrievals and further CYGNSS's ability to improve storm feature characterization.

To investigate this, all available storm observing Raw I/F tracks have been processed, and those relevant for the retrievals through the enforcement of a similar ± 30 min, relative to the mean along CYGNSS specular point track timestamp, CYGNSS/Storm separation, and a ± 200-km distance separation thresholds have been identified. Retrievals were then attempted

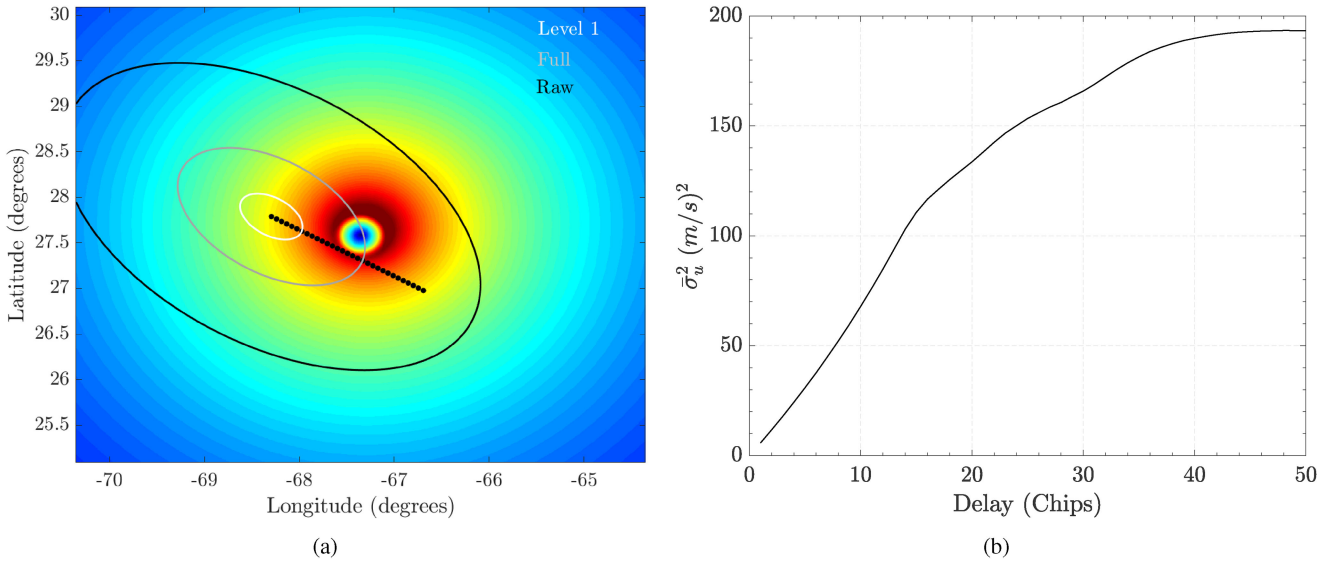

Fig. 8. Projections of spatial footprint of the three different CYGNSS DDM products. (a) Projection of spatial equivalent of maximum measurement delay extent for standard and special CYGNSS DDM products for a geometry resembling a Raw I/F mode downlink over hurricane Florence. (b) Variance of wind speed within measurement footprint at increasing delay extent. Locations of CYGNSS's specular points are indicated by the black scatters.

TABLE III
SUMMARY OF CYGNSS DATA PRODUCTS

Data Product	Total Delay	Surface Delay	Total Doppler	Comment
Compressed DDM	3.5 chips	∼1.75 chips	± 2.5 kHz	Standard product
Full DDM	32 chips	∼16 chips	± 5 kHz	Hurricanes Pre-Sept 2020
Full DDM, tracking point shifted	32 chips	∼28 chips	± 5 kHz	Hurricanes >Cat-3 Post-Sept 2020
Raw IF	Full Range (1023 chips)	Full Range (1023 chips)	No limit	Very high data rate, periodic collections

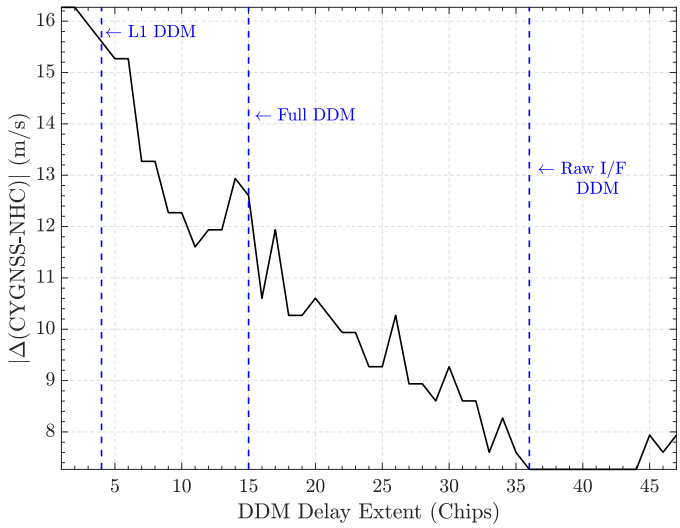

Fig. 9. Maximum hurricane wind retrieval error expressed as a function of maximum measurement delay extent using CYGNSS Raw I/F DDMs for a track observing hurricane Florence on DOY 254, 2018.

at varying delay extents ranging between 1 and 50 chips to investigate the dependence of retrieval error relative to delay extent. Sample results are shown in Fig. 9; a clear downward trend in error is observed as the measurement delay extent increases, thereby showing support for the value of measurements over larger delay extents in improving the sensing of cyclone maximum winds. Beyond roughly 46 chips, an upward trend in error is observed. This is not a general result and is specific to the track geometry analyzed as part of the example in Fig. 9 and arises due to the fact that delay bins corresponding to levels exceeding 46 chips fall into the lower gain portion of the receiver's antenna footprint such that no additional information on surface scattering is obtained at longer delays. Future investigation will aim to analyze error dependencies on storm properties and observation geometries in further detail.

VI. DISCUSSION

A number of areas through which further improvements in retrieval performance and capabilities may be achieved are discussed in this section.

The results presented in Section V highlight the sensitivity of retrieval performance to the set of model functions used to describe wind field distributions on the E2ES surface grid, clearly highlighting the need to have them accurately describe storm structure. While significant improvements in the quality of retrievals for weaker storms, relative to Willoughby-based estimates, are brought about by the use of the GAHM, it is emphasized that more realistic descriptions of storm structure it facilitates are only made possible through the ingestion of

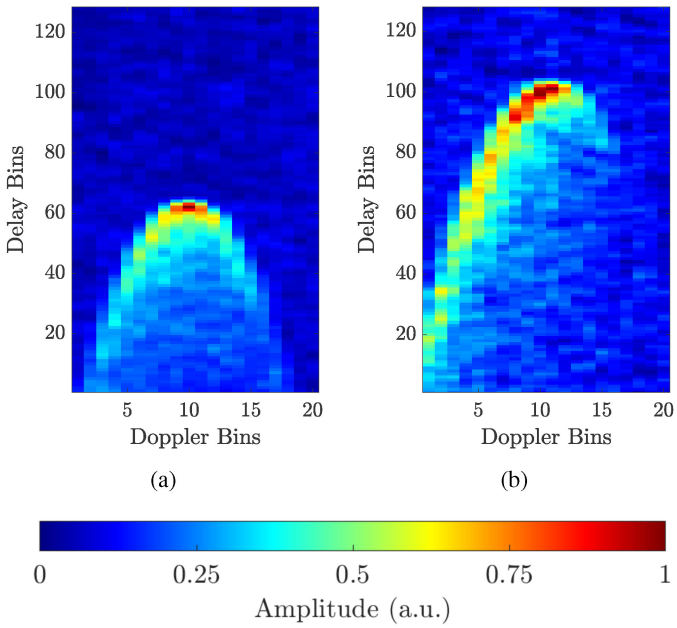

Fig. 10. Comparison of default Full DDM and tracking point shifted DDMs with varying delay extents. *a) Default Full DDM. (b) Tracking point shifted DDM.

a significantly increased number of ancillary parameters (described in Table I). To better improve the algorithm's readiness for retrievals in an operational capacity, it is desirable to limit the number of ancillary parameters required for retrievals, which may be achieved through further modifications of existing synthetic storm models. Analysis of correlations between those ancillary parameters, storm $V_{\max}$, and center latitude φ made available by the extensive Hurricane Database [44] record may prove instrumental in minimizing the number of required ancillary parameters.

Another consideration relevant to storm structures relates to storm "eyewall replacement" effects. As a storm develops into Cat. 4 and 5 hurricanes [45], the intensification of hurricane winds around the eyewall results in turbulent vortex breakdowns leading to the development of a new eye. As convection bands beyond the inner (original) eyewall reduces the amount of moisture surrounding it, the inner eyewall diminishes in size, while the outer (new) eyewall increases in diameter. At times, two eyewalls may exist or the location of the eyewall, and therefore the storm's center, may shift unpredictably, thereby directly impacting surface wind field distributions. Eyewall replacement effects are not captured by either the Willoughby model or the GAHM, and future improvements of this retrieval methodology should tackle the formulation of synthetic storm models that allow for multiple eyewall formations.

The results presented in Section V-D highlight the positive impacts of increased measurement delay on retrieval performance. Due to the increased datarate requirement of Raw I/F downlinks, they are not expected to become available with a sufficiently high frequency over hurricane observations. Another venue relates to expanding CYGNSS's Full DDM delay extent. The delay extent of a Full DDM comprises 128 bins with ≈0.25 chip sampling, half of which over the ocean are noise-only bins. Because the noise-only delay bins correspond to points, which fail to map onto the Earth's surface, their use is not expected to be relevant for $V_{\max}$ retrievals, and they are typically discarded, thereby limiting the Full DDM's maximum delay extent to 16 chips. The default open-loop tracking configuration for the Full DDMs is to target the ocean surface at the center delay bin, allowing for the large number of noise-only delay bins, which are used to accurately determine the measurement noise floor necessary for calibration. However, although the default delay location was generally sufficient given the small portion that is cropped out in the standard (Level-1) compressed DDM products, the excessive number of noise bins results in a loss of surface delay information at distances far from the specular point, which are of increased importance for the estimation of hurricane maximum winds. The increased utility of the extra delay bins prompted the design of a new operational mode, where the instrument open-loop tracking point is shifted to increase the number of surface delay bins, while providing a sufficient number of noise bins so as not to degrade the standard L1 calibration. This new "tracking point shifted" Full DDM tracks are commanded and collected over hurricanes that reach Cat-3 or higher, starting in September 2020. Examples of a default Full DDM and a tracking point-shifted DDM are shown in Fig. 10. The various CYGNSS data delay and Doppler extents are also summarized in Table III. Future works will report the retrieval performance achieved for measurements in this configuration.

VII. Conclusion

Cyclone maximum wind matched filter retrievals were demonstrated using tracks of Full and Raw I/F DDM measurements of the CYGNSS constellation. The impacts of using different storm models as part of the forward modeling procedure were analyzed. The two models incorporated as part of the E2ES forward modeling process include Willoughby model and GAHM. Optimal performance was shown to be achieved when the GAHM is used for storms with levels of development D_s is between ≤ 3 and the Willoughby model is used for the range $4 \leq D_s \leq 5$. Results from the method were shown for CYGNSS Full DDM cyclone overpasses for a total of 68 Full DDM retrievals spanning 18 storms over the period 2017–2020 with mean retrieval difference $\Delta_{\text{mean}} = 4.83$ m/s, RMSE $=$ 6.05 m/s, URMSE $=$ 6.05 m/s, bias is 0.09 m/s, and overall correlation $R = 92\%$. Relative to storm $V_{\max}$, error was found to be on average 11.11%. The success of the storm SSW retrieval methodology using Full DDMs motivates moving toward making their availability more frequent over storms.

The effects of measurement delay extent on retrieval error were also analyzed in the context of CYGNSS Raw I/F downlinks due to the facility of creating DDMs with arbitrary delay extents their use provides. A significant and near-monotonic decrease was observed in retrieval error associated with increased measurement extent. This was attributed to the increased information DDMs with longer "tails" provide about the storm's surface through sampling a larger portion of its structure within a single measurement.

ACKNOWLEDGMENT

The authors would like to thank NASA EOSDIS Physical Oceanography Distributed Active Archive Center (PO.DAAC) at the Jet Propulsion Laboratory, Pasadena, CA, USA, for making GNSS-R data derived from the CYGNSS constellation available. The authors would also like to thank Center for Satellite Application and Research (STAR) at NOAA-NESDIS, College Park, MD for making their Level-2 wind speed estimates derived from the CYGNSS constellation available.

REFERENCES

[1] X. Li, *Hurricane Monitoring With Spaceborne Synthetic Aperture Radar*. New York, NY USA: Springer, 2017.
[2] J. Hawkins, F. Turk, T. Lee, and K. Richardson, "Observations of tropical cyclones with the SSMIS," *IEEE Trans. Geosci. Remote Sens.*, vol. 46, no. 4, pp. 901–912, Apr. 2008.
[3] E. Im *et al.*, "Advanced geostationary radar for hurricane monitoring and studies," in *Proc. IEEE Radar Conf.*, 2004, pp. 307–311.
[4] B. Stiles *et al.*, "Optimized tropical cyclone winds from QuikSCAT: A neural network approach," *IEEE Trans. Geosci. Remote Sens.*, vol. 52, no. 11, pp. 7418–7434, Nov. 2014.
[5] S. Soisuvarn, Z. Jelenak, P. Chang, S. Alsweiss, and Q. Zhu, "CMOD5.H-A high wind geophysical model function for C-band vertically polarized satellite scatterometer measurements," *IEEE Trans. Geosci. Remote Sens.*, vol. 51, no. 6, pp. 3744–3760, Jun. 2013.
[6] M. Martin-Neira, "A passive reflectometry and interferometry system (PARIS): Application to ocean altimetry," *ESA J.*, vol. 17, pp. 331–355, Dec. 1993.
[7] V. Zavorotny and A. Voronovich, "Scattering of GPS signals from the ocean with wind remote sensing application," *IEEE Trans. Geosci. Remote Sens.*, vol. 38, no. 2, pp. 951–964, Mar. 2000.
[8] G. Foti, C. Gommenginger, and M. Srokosz, "First spaceborne GNSS-reflectometry observations of hurricanes from the U.K. TechDemoSat-1 mission," *Geophys. Res. Lett.*, vol. 44, no. 24, pp. 12358–123662017.
[9] M. Morris and C. Ruf, "Determining tropical cyclone surface wind speed structure and intensity with the CYGNSS satellite constellation," *J. Appl. Meteorol. Climatol.*, vol. 56, no. 7, pp. 1847–1865, 2017.
[10] M. Morris and C. Sampson, "CYGNSS-based TC characterization," in *Proc. CYGNSS Sci. Team Meeting*, Ann Arbor, MI USA, 2019.
[11] C. Bussy-Virat, C. Ruf, and A. Ridley, "Relationship between temporal and spatial resolution for a constellation of GNSS-R satellites," *IEEE J. Sel. Topics Appl. Earth Observ. Remote Sens.*, vol. 12, no. 1, pp. 16–25, Jan. 2019.
[12] C. Ruf *et al.*, "New ocean winds satellite mission to probe hurricanes and tropical convection," *Bull. Amer. Meteorol. Soc.*, vol. 97, no. 3, pp. 385–395, 2016.
[13] F. Said, S. Katzberg, and S. Soisuvarn, "Retrieving hurricane maximum winds using simulated CYGNSS power-versus-delay waveforms," *IEEE J. Sel. Topics Appl. Earth Observ. Remote Sens.*, vol. 10, no. 8, pp. 3799–3809, Aug. 2017.
[14] M. M. Al-Khaldi *et al.*, "Track-based cyclone maximum wind retrievals using the cyclone global navigation satellite system (CYGNSS) mission full DDMs," *IEEE J. Sel. Topics Appl. Earth Observ. Remote Sens.*, vol. 13, pp. 21–29, 2020, doi: 10.1109/JSTARS.2019.2946970.
[15] S. Gleason and C. Ruf, "Overview of the delay Doppler mapping instrument (DDMI) for the cyclone global navigation satellite systems mission (CYGNSS)," in *Proc. IEEE MTT-S Int. Microw. Symp.*, 2015, pp. 1–4.
[16] M. Clarizia and C. Ruf, "On the spatial resolution of GNSS reflectometry," *IEEE Geosci. Remote Sens. Lett.*, vol. 13, no. 8, pp. 1064–1068, Aug. 2016.
[17] M. Clarizia, C. Ruf, P. Jales, and C. Gommenginger, "Spaceborne GNSS-R minimum variance wind speed estimator," *IEEE Trans. Geosci. Remote Sens.*, vol. 52, no. 11, pp. 6829–6843, Nov. 2014.
[18] C. Ruf and R. Balasubramaniam, "Development of the CYGNSS geophysical model function for wind speed," *IEEE J. Sel. Topics Appl. Earth Observ. Remote Sens.*, vol. 12, no. 1, pp. 66–77, Jan. 2019.
[19] E. Uhlhorn, P. Black, J. Franklin, M. Goodberlet, J. Carswell, and A. Goldstein, "Hurricane surface wind measurements from an operational stepped frequency microwave radiometer," *Monthly Weather Rev.*, vol. 135, no. 9, pp. 3070–3085, 2007.
[20] M. P. Clarizia, V. Zavorotny, and C. Ruf, "Algorithm Theoretical Basis Document (ATBD): Level 2 Wind Speed Retrieval Technical Memo," 2018.
[21] D. Mayers and C. Ruf, "Tropical cyclone center fix using CYGNSS winds," *J. Appl. Meteorol. Climatol.*, vol. 58, no. 9, pp. 1993–2003, 2019.
[22] X. Li, J. Mecikalski and T. Lang, "A study on assimilation of CYGNSS wind speed data for tropical convection during 2018 January MJO," *Remote Sens.*, vol. 12, no. 8, 2020, Art. no. 1243.
[23] C. Ruf *et al.* "In-orbit performance of the constellation of CYGNSS hurricane satellites," *Bull. Amer. Meteorol. Soc.*, vol. 100, no. 10, pp. 2009–2023, 2019.
[24] R. Balasubramaniam and C. Ruf, "Neural network based quality control of CYGNSS wind retrieval," *Remote Sens.*, vol. 12, no. 17, 2020, Art. no. 2859.
[25] T. Wang, C. Ruf, B. Block, D. McKague, and S. Gleason, "Design and performance of a GPS constellation power monitor system for improved CYGNSS L1B calibration," *IEEE J. Sel. Topics Appl. Earth Observ. Remote Sens.*, vol. 12, no. 1, pp. 26–36, Jan. 2019.
[26] S. Gleason, A. O'Brien, A. Russel, M. M. Al-Khaldi, and J. T. Johnson, "Geolocation, Calibration and Surface Resolution of CYGNSS GNSS-R land observations," *Remote Sens.*, vol. 12, 2020, Art. no. 1317.
[27] S. Gleason, C. Ruf, A. O'Brien, and D. McKague, "The CYGNSS level 1 calibration algorithm and error analysis based on on-orbit measurements," *IEEE J. Sel. Topics Appl. Earth Observ. Remote Sens.*, vol. 12, no. 1, pp. 37–49, Jan. 2019.
[28] A. O'Brien, S. G. Gleason, and J. T. Johnson, "The CYGNSS end-to-end simulator," in *Proc. GNSS R Workshop*, Postdam, Germany, May 2017.
[29] A. O'Brien and J. T. Johnson, "Comparing the CYGNSS simulator forward scattering model with TDS-1 and CYGNSS on-orbit observations," *IEEE Int. Geosci. Remote Sens. Symp.*, Fort Worth, TX, USA, Jul. 2017, pp. 2657–2658.
[30] S. Katzberg, J. Dunion, and G. Ganoe, "The use of reflected GPS signals to retrieve ocean surface wind speeds in tropical cyclones," *Radio Sci.*, vol. 48, no. 4, pp. 371–387, 2013.
[31] S. Katzberg, O. Torres, and G. Ganoe, "Calibration of reflected GPS for tropical storm wind speed retrievals," *Geophys. Res. Lett.*, vol. 33, no. 18, pp. 8602–8607, 2006.
[32] G. Holland, "An analytic model of the wind and pressure profiles in hurricanes," *Monthly Weather Rev.*, vol. 108, no. 8, pp. 1212–1218, 1980.
[33] G. Holland, J. Belanger and A. Fritz, "A revised model for radial profiles of hurricane winds," *Monthly Weather Rev.*, vol. 138, no. 12, pp. 4393–4401, 2010.
[34] C. Deppermann, "Notes on the origin and structure of philippine typhoons," *Bull. Amer. Meteorol. Soc.*, vol. 28, no. 9, pp. 399–404, 1947.
[35] R. W. Schloemer, "Analysis and synthesis of hurricane wind patterns over lake okeechobee," U.S. Dept. Commerce Weather Bur., Washington, DC, USA, Tech. Rep. 31, 1954.
[36] P. Ruiz-Salcines, P. Salles, L. Robles-Diaz, G. Diaz-Hernandez, A. Torres-Freyermuth, and C. Appendini, "On the use of parametric wind models for wind wave modeling under tropical cyclones," *Water*, vol. 11, no. 10, 2019, Art. no. 2044.
[37] Y. Tsai, T. Wu, C. Lin, S. Lin, E. Yen, and C. Lin, "Discrepancies on storm surge predictions by parametric wind model and numerical weather prediction model in a semi-enclosed bay: Case study of typhoon Haiyan," *Water*, vol. 12, no. 12, 2020, Art. no. 3326.
[38] H. Willoughby and M. Rahn, "Parametric representation of the primary hurricane vortex. Part I: Observations and evaluation of the Holland (1980) model," *Monthly Weather Rev.*, vol. 132, no. 12, pp. 3033–3048, 2004.
[39] H. Willoughby, R. Darling, and M. Rahn, "Parametric representation of the primary hurricane vortex. Part II: A new family of sectionally continuous profiles," *Monthly Weather Rev.*, vol. 134, no. 4, pp. 1102–1120, 2006.
[40] J. Gao, "On the surface wind stress for storm surge modeling," Ph.D. dissertation, Dept. Mar. Sci., Univ. North Carolina at Chapel Hill, Chapel Hill, NC, USA, 2018.
[41] A. T. Cox and V. J. Cardone, "20 years of operational forecasting at oceanweather," in *Proc. 7th Int. Workshop Wave Hindcasting Forecasting*, 2002, pp. 21–25.
[42] J. Gao, R. Leuttich, and J. Fleming, "Development and initial evaluation of a generalized asymmetric tropical cyclone vortex model in ADCIRC," in *Proc. ADCIRC Users Group Meeting*, Vicksburg, MS, USA, 2013.
[43] *The Saffir/Simpson Hurricane Scale, NOAA's National Climatic Data Center*, Asheville, NC, USA, 2020.

[44] P. Chylek and G. Lesins, "Multidecadal variability of atlantic hurricane activity: 1851–2007," *J. Geophys. Res.*, vol. 113, no. 22, 2008, Art. no. D22106.
[45] R. Houze, S. Chen, B. Smull, W. Lee, and M. Bell, "Hurricane intensity and eyewall replacement," *Science*, vol. 315, no. 5816, pp. 1235–1239, 2007.

Mohammad M. Al-Khaldi (Member, IEEE) received the bachelor's degree in electrical engineering from the American University of Sharjah, Sharjah, United Arab Emirates, in 2015, the M.S. degree in electrical engineering from Texas A&M University, College Station, TX, USA, in 2017, the M.S. and Ph.D. degrees in electrical and computer engineering from The Ohio State University, Columbus, OH, USA, in 2019 and 2020, respectively.

He is currently a Postdoctoral Researcher with the Constellation Observing System for Meteorology, Ionosphere, and Climate Program, University Corporation for Atmospheric Research, Boulder, CO, USA. His research interests include applied electromagnetics, rough surface scattering, and spaceborne remote sensing.

Stephen J. Katzberg was born in Clinton, SC, USA, in 1943. He received the B.S. degree from the Massachusetts Institute of Technology, Cambridge, MA, USA, in 1965, and the M.S. and Ph.D. degrees from the University of Virginia, Charlottesville, VA, USA, in 1967 and 1970, respectively, all in electrical engineering.

He has worked nearly exclusively with the NASA Langley Research Center, Hampton, VA, for 40-some odd years and is currently a Distinguished Research Associate. He is also an Adjunct Professor with South Carolina State University, Orangeburg, SC, USA.

Joel T. Johnson (Fellow, IEEE) received the bachelor's degree in electrical engineering from the Georgia Institute of Technology, Atlanta, GA, USA, in 1991, and the S.M. and Ph.D. degrees from the Department of Electrical Engineering and Computer Science, Cambridge, MA, USA, in 1993 and 1996, respectively.

He is currently a Professor with the ElectroScience Laboratory, Department of Electrical and Computer Engineering, The Ohio State University, Columbus, OH, USA. His current research interests include the areas of microwave remote sensing, propagation, and electromagnetic wave theory.

Dr. Johnson is a member of commissions B and F of the International Union of Radio Science (URSI), Tau Beta Pi, Eta Kappa Nu, and Phi Kappa Phi. He received the 1993 Best Paper Award from the IEEE Geoscience and Remote Sensing Society, was named an Office of Naval Research Young Investigator, the National Science Foundation Career Awardee, the PECASE Award Recipient in 1997, and was recognized by the U.S. National Committee of URSI as a Booker Fellow in 2002. He served as Technical Program Co-Chair for the 2017 International Geoscience and Remote Sensing Symposium. He has served as an Associate Editor for the IEEE TRANSACTIONS ON GEOSCIENCE AND REMOTE SENSING since 2000. He is also a Past Chair of the GRSS Technical Committee on Frequency Allocations in Remote Sensing.

Younghun Kang received the bachelor's degree in mathematics from Dongguk University, Seoul, South Korea, in 2015, and the M.S. degree in computational science and engineering from Yonsei University, Seoul, in 2017. He is currently working toward the Ph.D. degree with the Department of Civil, Environmental and Geodetic Engineering, The Ohio State University, Columbus, OH, USA.

He is currently a Graduate Research Associate with the Department of Civil, Environmental and Geodetic Engineering and the Computational Hydrodynamics and Informatics Lab, The Ohio State University. His research interests include numerical simulation and validation studies for storm surge prediction and analysis of finite-element methods with emphasis on discontinuous Galerkin methods.

Ethan J. Kubatko received the B.S. degree in civil engineering from the Pennsylvania State University, University Park, PA, USA, in 1997, and the Ph.D. degree in civil engineering from the University of Notre Dame, Notre Dame, IN, USA, in 2006.

He is currently an Associate Professor with the Department of Civil, Environmental and Geodetic Engineering, The Ohio State University, Columbus, OH, USA. His primary research interests include the development, implementation, analysis, and application of computational models for fluid flow and transport processes. Much of his recent work has focused on hurricane storm surge modeling.

Scott Gleason (Senior Member, IEEE) received the B.S. degree in electrical and computer engineering from the State University of New York at Buffalo, Buffalo, NY, USA, in 1991, the M.S. degree in engineering from Stanford University, Stanford, CA, USA, in 1999, and the Ph.D. degree in applied physics from the University of Surrey, Surrey, U.K., in 2007.

He is a Project Scientist III with the University Corporation for Atmospheric Research, Boulder, CO, USA. He is a Co-Investigator on the science team and Instrument Scientist for the NASA CYGNSS mission. He has worked in the areas of astronautics, remote sensing, and global navigation satellite systems for more than 20 years, including at NASA's Goddard Space Flight Center, Stanford's GPS Laboratory, Surrey Satellite Technology Limited, Concordia University, and the National Oceanography Centre, Southampton, U.K.